CHEMISTRY OF MATERIALS

Article

pubs.acs.org/cm

Self-templating Scheme for the Synthesis of Nanostructured Transition-Metal Chalcogenide Electrodes for Capacitive Energy Storage

Chuan Xia and Husam N. Alshareef*

Materials Science and Engineering, King Abdullah University of Science and Technology (KAUST), Thuwal 23955-6900, Saudi Arabia

Supporting Information

ABSTRACT: Because of their unique structural features including well-defined interior voids, low density, low coefficients of thermal expansion, large surface area and surface permeability, hollow micro-/nanostructured transition-metal sulfides with high conductivity have been investigated as a new class of electrode materials for pseudocapacitor applications. Herein, we report a novel self-templating strategy to fabricate well-defined single- and double-shell $NiCo_2S_4$ hollow spheres, as a promising electrode material for pseudocapacitors. The surfaces of the $NiCo_2S_4$ hollow spheres consist of self-assembled two-dimensional mesoporous nanosheets. This unique morphology results in a high specific capacitance (1263 F g^{-1} at 2 A g^{-1}), remarkable rate performance (75.3% retention of initial capacitance from 2 to 60 A g^{-1}), and exceptional reversibility with a cycling efficiency of 93.8% and 87% after 10 000 and 20 000 cycles, respectively, at a high current density of 10 A g^{-1}. The cycling stability of our ternary chalcogenides is comparable to carbonaceous electrode materials, but with much higher specific capacitance (higher than any previously reported ternary chalcogenide), suggesting that these unique chalcogenide structures have potential application in next-generation commercial pseudocapacitors.

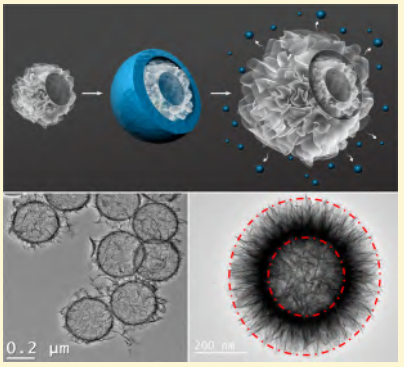

1. INTRODUCTION

The fact that fossil fuels will ultimately be depleted has increased efforts aimed at using renewable energy sources in our daily life. Yet, the intermittency and unstable nature of some renewable energy sources such as solar and wind energy has driven the demand for energy storage devices.[1−4] Batteries, which are expected to feature prominently in any renewable energy system, suffer from low power density and short cycling stability,[1,5,6] which can limit their utilization. In this case, supercapacitors, which offer a much longer life cycle, higher power density, and safer operation than batteries, can be used to complement batteries, where high power is needed. Supercapacitors can be generally classified into two types, depending on the underlying energy storage mechanism. One type is the electrical double-layer capacitors (EDLCs), which store electrical energy by charge accumulation at the electrode/electrolyte interface. The other type is pseudocapacitors, which are based on the fast and reversible redox reactions at the surface of electro-active materials, thus offering much higher specific capacitance and energy density than EDLCs.[1,7−9] Previously developed pseudocapacitors have been based on transition-metal oxides, hydroxides, and conducting polymers which invariably suffer from either low conductivity or poor electrochemical stability, largely limiting their applications.[10−14] Therefore, it is imperative to create alternative pseudocapacitive materials with low cost, desirable electrical conductivity, highly porous structure, high specific surface area, desirable ionic permeability, large capacitance, and good electrochemical stability.[15,16]

Because of their unique structural features including well-defined interior voids, low density, low coefficients of thermal expansion, large surface area, and surface permeability, hollow micro-/nanostructured binary transition-metal sulfides such as nickel sulfide and cobalt sulfide have been widely investigated as a new class of pseudocapacitive electrode materials.[17−22] Unfortunately, the previous reports showed either relatively low specific capacitance or poor rate capability, as well as quite limited enhancement of cycle life. In addition, the template-based methods always required an additional time-consuming step to remove the template.

Very recently, it has been reported that mixed transition-metal sulfides, particularly nickel cobalt sulfides ($NiCo_2S_4$), showed excellent properties when used as pseudocapacitive material. These results are due to the intrinsic stability, higher electrical conductivity (~100 times as high as that of $NiCo_2O_4$ and much higher than those of the binary sulfides), and richer redox reactions than the corresponding single-component sulfides, in much the same way as $NiCo_2O_4$ to the corresponding single-component oxides.[23−26] In addition, it has been well-demonstrated that an outer protection layer is important to stabilize the nanostructured ultrathin hollow

Received: March 26, 2015
Revised: June 10, 2015
Published: June 11, 2015

DOI: 10.1021/acs.chemmater.5b01128
Chem. Mater. 2015, 27, 4661−4668

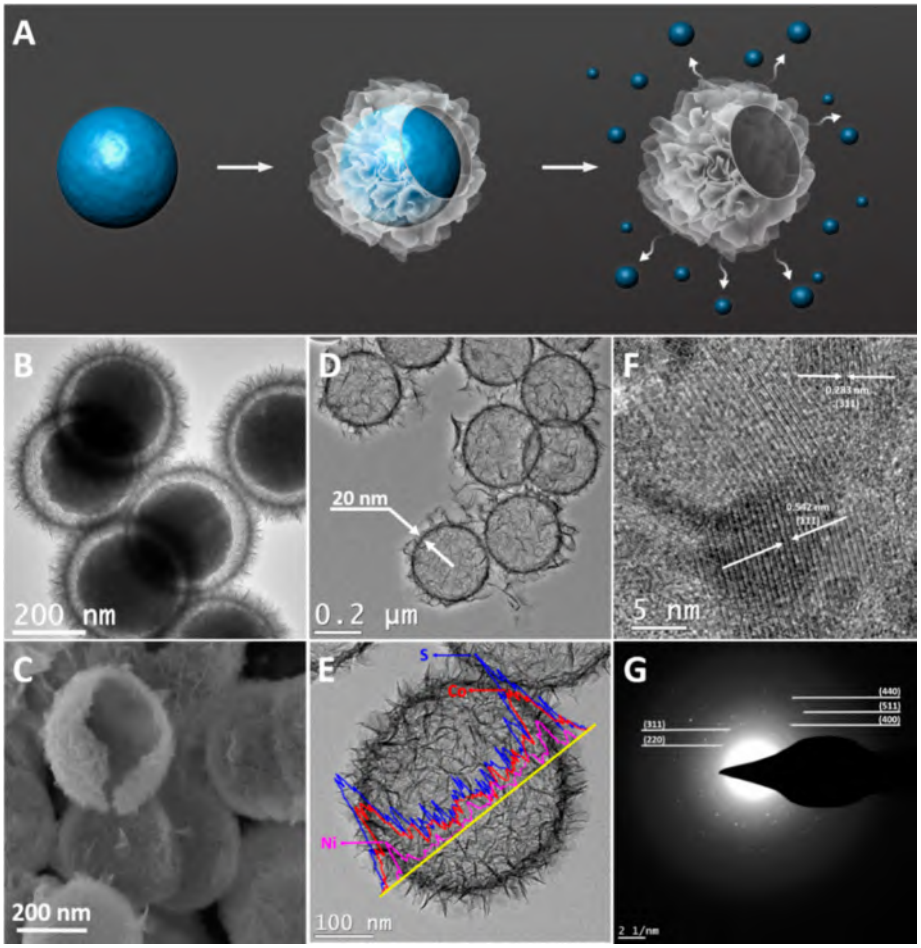

Figure 1. (A) Schematic of the synthesis of $NiCo_2S_4$ hollow spheres. (B) TEM image of the 350 nm silica based precursor. (C) FESEM and (D) TEM images of 300 nm $NiCo_2S_4$ hollow sphere obtained from Ni−Co hydrosilicate precursor. (E) EDS-STEM line scan of 300 nm $NiCo_2S_4$ hollow sphere; the purple, blue, and red lines represent counts of nickel, cobalt, and sulfur signals along the solid yellow line, respectively. (F) HRTEM image and (G) the corresponding selected-area electron diffraction pattern of 300 nm $NiCo_2S_4$ hollow sphere.

spheres.[27−29] In this sense, double-shell hollow structures of $NiCo_2S_4$ with protection of outer layer, large surface area, highly porous structure, and desirable ionic permeability may be an excellent potential pseudocapacitive material. To date, while binary transition-metal sulfides have been well-established, it remains a challenge to fabricate well-defined hollow structures of ternary transition-metal sulfides such as $NiCo_2S_4$.

In this paper, we report a self-templating strategy to controllably fabricate well-defined $NiCo_2S_4$ (NCS) single- and double-shell hollow spheres (HS) for high-performance pseudocapacitors. The size of the interior void of these hollow spheres could be easily tuned by tailoring the size of the starting silica template, generating significant difference in electrochemical performance. Even more, the size effect of template and morphology-dependent enhancement of pseudocapacitive performance is demonstrated.

2. EXPERIMENTAL SECTION

2.1. Synthesis of Silica Template. Monodisperse SiO_2 solid spheres with varied size were prepared using a modified Stöber process.[30] In a typical synthesis of ∼750 nm silica, 6 mL of TEOS was rapidly added into a mixture of 62 mL of ethanol and 12 mL of ammonia (30−30%). The mixture was stirred at 360 rpm for 1 h, repeatedly washed with deionized (DI) water and ethanol. To acquire ∼490 and ∼380 nm of silica, typically 9 or 3 mL of ammonia (30−33%) as catalyst was added into the starting reagents containing 4.5 mL of TEOS, 24.75 mL of H_2O, and 61.75 or 67.75 mL of ethanol, respectively. Afterward, this mixture was kept at room temperature while stirring at 360 rpm for 2 h, followed by washing and drying. Particularly, ∼100 nm silica was obtained from a mixture of 2 mL of TEOS, 8 mL of ammonia (30−33%), 75 mL of methanol, and 10 mL of DI water. After the mixture was stirred at room temperature under 360 rpm for 2, the products were washed and dried in air.

2.2. Synthesis of Ni−Co Hydrosilicate Precursor. Typically, 5 mmol of silica solid-sphere template with different diameters (Supplemental Figure S16) or commercial silica nanoparticles were dispersed in 40 mL of DI water, followed by the addition of 16.7 mmol of urea, 0.3 mmol of $Ni(NO_3)_2{\cdot}6H_2O$, and 0.6 mmol of $Co(NO_3)_2{\cdot}6H_2O$. After vigorous stirring at room temperature for 0.5 h, the thoroughly mixed solution was kept at 105 °C for 12 h under mild stirring. After cooling down naturally, the product was centrifuged and washed.

2.3. Synthesis of $NiCo_2S_4$ Single-Shell Hollow Spheres and $NiCo_2S_4$ Nanosheets. As-prepared precursor (0.1 g) was redispersed into 40 mL of DI water, following by the addition of 0.3 g of Na_2S. After vigorous stirring for 15 min, this solution was subsequently transferred into a Teflon-lined autoclave and kept at 160 °C for 12 h. The final product was washed and dried in a vacuum at 60 °C. After drying, the as-prepared powder was annealed under N_2 atmosphere at 300 °C for 0.5 h prior to X-ray diffraction measurement to determine the crystal phase.

2.4. Synthesis of $NiCo_2S_4$ Double-Shell Hollow Spheres. The core−shell NCS@SiO_2 structure was prepared through a versatile

DOI: 10.1021/acs.chemmater.5b01128
Chem. Mater. 2015, 27, 4661−4668

Stöber sol−gel method as follows.[30,31] Sixty milligrams of NCS HS was redispersed into 280 mL of ethanol, followed by the addition of 70 mL of DI water and 5 mL of ammonia (30−33%). Afterward, 4 mL of TEOS was added dropwise in 10 min, and the reaction was kept at room temperature for 12 h under mild stirring to obtain the NCS@SiO_2 core−shell products. Then, NCS@Ni-Co precursors were obtained by repeating section 2.2. Next, 0.1 g of the resultant core−shell structure was added into 40 mL of DI water which contained 0.3 g of Na_2S. After being thoroughly mixed, this solution was kept at 160 °C for 12 h in the autoclave. After centrifugation and washing, the resultant was annealed under N_2 atmosphere at 300 °C for 0.5 h prior to X-ray diffraction measurement to determine the crystal phase.

2.5. Materials Characterization. The morphology and microstructure were investigated by scanning electron microscopy (SEM; Nova Nano 630, FEI) and transmission electron microscopy [TEM; Titan 80-300 kV (ST) TEM, FEI], and the elemental presence and composition were identified using energy-dispersive X-ray spectroscopy (EDS) and XPS analysis (Kratos AXIS Ultra DLD). The XRD measurement was conducted on a powder X-ray diffraction (XRD) system (Bruker, D8 ADVANCE) equipped with Cu Kα radiation (λ = 0.15406 nm). Brunauer, Emmett, and Teller (BET) surface areas of the samples were determined using surface area and porosimetry system "Micromeritics" (ASAP 2420) at 77 K. Before measurements, the samples were dried at 70 °C for 10 h in a vacuum oven and then degassed at 200 °C for 6 h until the vacuum was less than 2 μm Hg.

2.6. Electrochemical Measurements. The electrochemical tests were carried out at room temperature in three-electrode (half-cell) configurations with $NiCo_2S_4$ as a working electrode, a Pt wire as the counter electrode, and saturated calomel electrode as the reference electrode. The working electrodes with a mass loading of ∼1 mg cm^{-2} were prepared by coating the active $NiCo_2S_4$, acetylene black and polyvinylidene flouride (PVDF) in a weight ratio of 7:2:1 on the carbon cloth. One molar KOH was used as electrolyte for all measurements.

The specific capacitance was then calculated from the galvanostatic charge−discharge (CD) curves as

$$C = \frac{I}{m\frac{\Delta V}{\Delta t}}$$

where m is the total mass loading of the electrode, I is the constant current for charge−discharge, and $\Delta V/\Delta t$ is the slope of the discharge curve.[32]

3. RESULTS AND DISCUSSION

As schematically illustrated in Figure 1A, the synthesis strategy of $NiCo_2S_4$ hollow spheres can be generally described as the hydrolysis−sulfidation process. First, as-prepared 350 nm silica spheres were used as a template and raw material to prepare nickel cobalt silicate hydroxide precursor through a facile hydrolysis process at 105 °C (see Experimental Section for details). As shown in Figure S1 of the Supporting Information, the color of starting materials changes from light gray to pink after the hydrolysis process, demonstrating the formation of nickel cobalt hydrosilicate, which originates from the coprecipitation of Ni^{2+} and Co^{2+} cations on the surface of monodispersed silica nanospheres in an alkaline solution.[33] To investigate the phase and structure at various stages of the reaction, X-ray diffraction (XRD) patterns were recorded. The typical XRD pattern of the precursor (Figure S2) showed one broad diffraction peak around 23°, which can be assigned to the amorphous silica phase. In addition, the two peaks around 34° and 60° could be assigned to the (200) and (600) planes of crystalline $(Ni,Co)_3Si_2O_5(OH)_4$ phase, although the exact crystal structure remains unsolved.[34] The as-prepared precursor retains the original morphology of the silica template with a diameter of 300 nm, as clearly shown in Figure 1B and Figure S3. The corresponding high-angle annular dark-field scanning transmission electron microscopy (HAADF-STEM) image and elemental analysis also reveal the core−shell structure and the successful formation of Ni−Co hydrosilicate of our $(Ni,Co)_3Si_2O_5(OH)_4$@SiO_2 precursor (Figure S4). The obvious empty gap between the inner silica core and the outer Ni−Co hydrosilicate shell shows that the silica not only serves as a template but also gets involved in the hydrolysis reaction. Next, the well-defined $NiCo_2S_4$ hollow spheres (HS) were derived from the precursor via a facile in situ sulfidation process using Na_2S as sulfur source. During the chemical transformation process, the silica cores are etched simultaneously by NaOH, which is released from the hydrolysis of Na_2S, eliminating the need for an additional etching step to remove the silica template. The crystal phase and structure of the product after sulfidation were investigated by XRD. All diffraction peaks (Figure S2) can be assigned to thiospinel $NiCo_2S_4$ without any noticeable second phases.

Figure 1C,D reveals the morphology and microstructure of the as-obtained $NiCo_2S_4$ hollow spheres (black solution in Figure S1). Interestingly, these hierarchical hollow spheres are entirely self-assembled from ultrathin mesoporous $NiCo_2S_4$ nanosheets with a thickness of a few nanometers (Figure S5),[20] thereby resulting in large surface-to-volume ratio and highly mesoporous structure. Such a structure offers a large interfacial area between the electroactive $NiCo_2S_4$ and the electrolyte ions, and short diffusion paths for fast ionic diffusion, which is highly desirable for pseudocapacitors. From the close-up STEM images in Figure S6, an outer rough surface of the hollow spheres, consisting of curved nanosheets, with a thickness around 20 nm, can be discerned. The lattice fringes with different orientations shown in Figure 1F suggest that the as-obtained $NiCo_2S_4$ HS is polycrystalline in nature, which is confirmed by the corresponding selected-area electron diffraction (SAED) pattern in Figure 1G.

Energy-dispersive X-ray spectroscopy (EDS) and X-ray photoelectron spectroscopy (XPS) were carried out to provide further insight into the hollow interior as well as the chemical composition and oxidation states of the as-prepared $NiCo_2S_4$ HS. Figure 1E shows the EDS-STEM line scans of the 300 nm $NiCo_2S_4$ HS for nickel, cobalt, and sulfur. The profiles of Ni, Co, and S have a broad spectrum throughout the entire diameter but are more prominent at the boundary region, corresponding to the hollow nature of the of $NiCo_2S_4$ spheres. Figure 2 shows the typical energy-filtered transmission electron microscopy (EFTEM) elemental mapping for 300 nm $NiCo_2S_4$ HS. A uniform distribution of the elements Ni, Co, and S on the surface of the hollow sphere is clearly visible, further demonstrating the successful preparation of thiospinel $NiCo_2S_4$. High-resolution XPS spectra of Co 2p, Ni 2p, and S 2p core levels have been recorded and are shown in Figure S7, which matches well with those obtained for ternary $NiCo_2S_4$.[23−25] From the survey scans of XPS spectrum (Figure S7A), the presence of a small amount of Si is likely to be the amorphous silicate residue.[20] Furthermore, N_2 adsorption/desorption measurements (Figure S8) demonstrate that the $NiCo_2S_4$ HS themselves are mesoporous in nature with uniform pores of around 3 nm, possessing a large BET surface area of 122 m^2 g^{-1}. Such highly mesoporous HS structure with exceptional surface permeability for electrolyte ions is the ideal morphology for pseudocapacitor applications because it can enhance electrochemical surface reactions.

DOI: 10.1021/acs.chemmater.5b01128
Chem. Mater. 2015, 27, 4661−4668

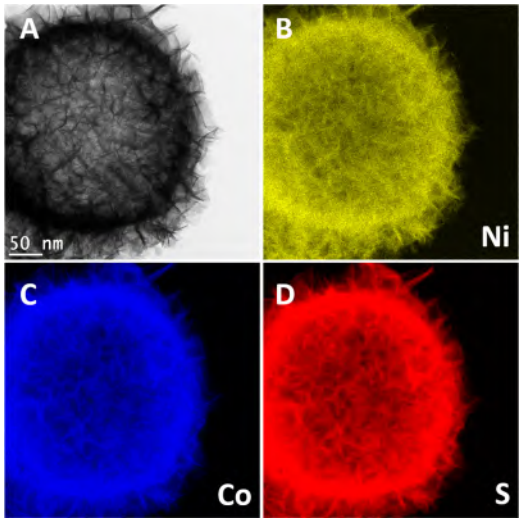

Figure 2. (A) Typical transmission secondary electron image of the $NiCo_2S_4$ hollow sphere; and the corresponding energy-filtered transmission electron microscopy (EFTEM) elemental mapping of (B) nickel, (C) cobalt, and (D) sulfur, respectively.

It has been reported that the sphere size can significantly affect the electrochemical performance for nanostructured hollow spheres in other material systems.[35,36] We have therefore prepared various sizes of $NiCo_2S_4$ hollow spheres (700, 450, 300, and 100 nm in diameter) using different sizes of silica templates (see Experimental Section for details), henceforth referred to as 700 nm NCS through 100 nm NCS. The electrochemical properties of different sizes of $NiCo_2S_4$ HSs were investigated by three-electrode configuration in 1.0 M KOH solution. Figure 3A,B shows the cyclic voltammetry (CV) and galvanostatic discharge curves obtained at 20 mV s^{-1} and 10 A g^{-1} for all samples, respectively. One pronounced pair of peaks can be observed in the representative CV curves, clearly revealing the pseudocapacitive characteristics of these materials.[25,37,38] The formation of the broad redox peaks can be attributed to the highly reversible Faradaic reactions of Ni^{2+}/Ni^{3+} and $Co^{2+}/Co^{3+}/Co^{4+}$ pairs with electrolyte anions OH^-, according to the following equation:[26,39]

$$NiCo_2S_4 + 2OH^- \leftrightarrow NiS_{4-2x}OH + 2CoS_xOH + 2e^-$$

$$CoS_xOH + OH^- \leftrightarrow CoS_xO + H_2O + e^-$$

Moreover, multiple distinct voltage plateaus are manifested in the galvanostatic discharge profiles which suggest the presence of reversible redox reactions, consistent with the electrochemical behavior of the CV curves. The small voltage (IR) drop observed in the galvanostatic discharge curves is attributed to the high conductivity of $NiCo_2S_4$,[23] resulting in low equivalent series resistances (ESR), which results in high pseudocapacitive performance. At the same scan rate of 20 mV s^{-1}, it is obvious that the integrated area of CV curves (from 700 nm NCS to 100 nm NCS) first increases and then decreases, suggesting a strong influence of the sphere size on electrode capacitance. The galvanostatic discharge curves also illustrate varied discharge periods at current density of 10 A g^{-1}, matching with the results from CV measurements. Figure 3C presents the specific capacitance for all studied samples. It is clear that 300 nm NCS HS has higher specific capacitance (997 F g^{-1} at 2 A g^{-1}) than the other samples (901, 929, and 745 F g^{-1} for 700, 450, and 100 nm NCS at 2 A g^{-1}, respectively). Figure 3D clearly shows that the pseudocapacitive performance of our $NiCo_2S_4$ hollow spheres is strongly correlated to the diameter size, especially for the cycling stability performance (Figure 3E); similar phenomena of size-dependent electrochemical performance were also observed in battery materials such as SnO_2 hollow spheres.[35] The sphere size effect on the $NiCo_2S_4$ performance can be explained by the following factors. First, the BET surface area of the four studied hollow sphere sizes initially increases from 700 to 300 nm NCS and then decreases dramatically from 300 to 100 nm NCS, a fact that has been revealed by the BET measurement (Figure S8). The larger surface area can offer a higher concentration of electrochemi-

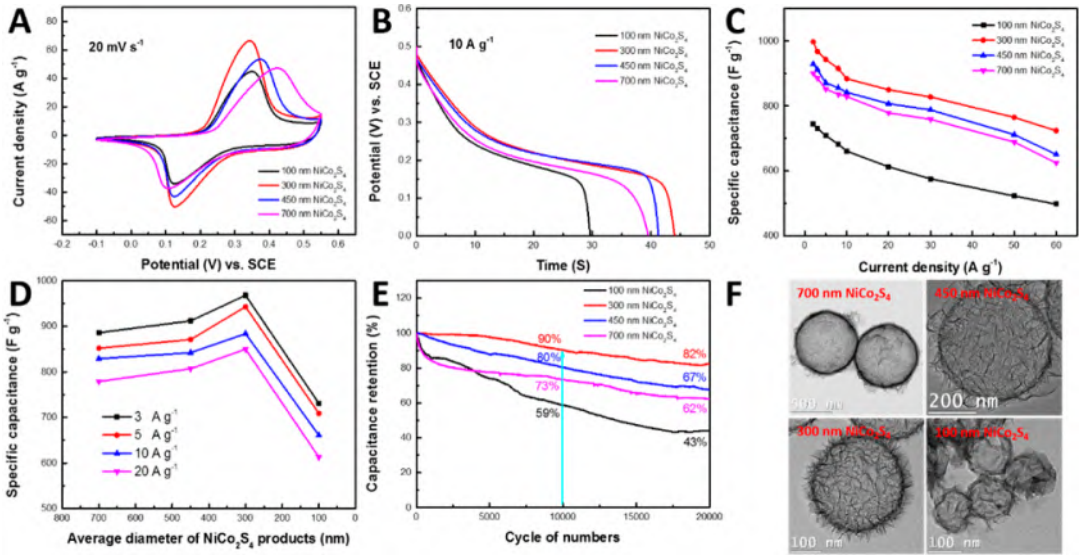

Figure 3. (A) Cyclic voltammetry curves at the same scan rate of 20 mV s^{-1}; (B) galvanostatic discharge profiles at the same current density of 10 A g^{-1}; and (C) summary of specific capacitance as a function of current density of all studied samples. (D) Summary of specific capacitance as a function of average diameter of $NiCo_2S_4$ hollow sphere. (E) Cycling stability performance at current density of 10 A g^{-1} and (F) representative TEM images of all as-prepared samples.

DOI: 10.1021/acs.chemmater.5b01128
Chem. Mater. 2015, 27, 4661−4668

cally active sites, larger interfacial area between the electroactive materials and the electrolyte ions, and shorter diffusion paths for fast ionic diffusion, all of which can promote the electrochemical performance.[40] Second, it is well-known that the spherical shell geometry is capable of withstanding extreme stresses, and the maximum tensile stress in a hollow Si sphere is ~5 times lower than that of a solid Si sphere of equal volume, during electrochemical reaction.[35,41,42] Therefore, the larger size $NiCo_2S_4$ HS is more fragile during the long-term cycling measurement. Hence, the smaller sized silica template results in better $NiCo_2S_4$ HS integrity, which can endure the large volume change without pulverization.[35] Third, as mentioned above, the silica in this case is used as a starting material and plays the role of a self-dissolving template. The empty gap between shells shown in Figure 1B successfully demonstrates the partial dissolution of silica template as it participates in the hydrolysis reaction. As illustrated in Figure 3F, and Figure S9, the 700, 450, and 300 nm silica spheres are large enough to act as template, resulting in a uniform morphology and well-defined $NiCo_2S_4$ HS. Yet, the data appears to show that the 100 nm silica template might be too small to support the formation of an outer shell. Thus, the morphology of the final product prepared by templating with 100 nm silica (Figure 3F and Figure S10) is a mixture of random quasi-hollow spheres and nanosheets with the lowest BET surface area among all samples. These factors result in the worst electrochemical performance and worst capacitance retention for the 100 nm NCS. This particular morphology is full of defects and cracks, which can more easily lead to pulverization of the $NiCo_2S_4$ electrode into small fragments. Thus, we can conclude that there is a critical sphere size for obtaining good electrochemical performance for our $NiCo_2S_4$ HS electrodes. The optimized 300 nm NCS HS electrode exhibits a high specific capacitance of 997 F g^{-1} at 2 A g^{-1}, good rate performance, and impressive long cycle life at high current density of 10 A g^{-1} (retention 90.3% and 82% after 10 000 and 20 000 cycles, respectively). This result is one of the most stable pseudocapacitive materials among the reported materials in the literature.

As we have demonstrated in the previous section, the $NiCo_2S_4$ hollow sphere electrodes made using 300 nm silica sacrificial template display optimal electrochemical performance. Notwithstanding the remarkable performance, the cycle life of 300 nm NCS HS need to be competitive with commercial carbonaceous material electrodes. Recognizing that an outer protection layer can be used to stabilize hollow electrode structures, we decided to study the effect of placing a second chalcogenide shell around the first one. Hence, a second highly conductive $NiCo_2S_4$ protection shell was directly coated on the first 300 nm NCS hollow sphere, resulting in a $NiCo_2S_4$ double-shell structure. As illustrated in Figure 4A, a TEOS (tetraethyl orthosilicate)-driven silica was used to deposit a uniform and conformally deposited layer on the surface of 300 nm NCS hollow spheres via a versatile Stöber sol–gel method.[27,31] Afterward, the $NiCo_2S_4$ outer shell was formed using the same hydrolysis–sulfidation process (see Experimental Section for details). Figure 4B,C reveals TEM images with different magnifications for 300 nm NCS HS@SiO_2 core–shell structure. Obviously, the NCS HS retains the 300 nm hollow interior with around 100 nm second shell of silica. After the same hydrolysis–sulfidation process, the dense silica outer shell transforms into highly porous nanosheet arrays on the surface, with a thickness of around 150 nm, as shown in Figure 4D,E and Figure S11. XRD measurement shows again single

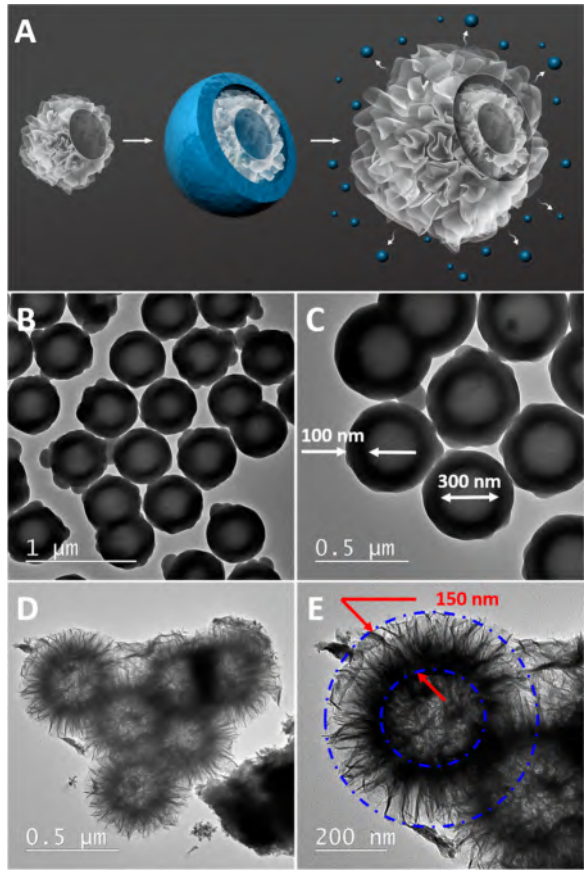

Figure 4. (A) Schematic illustration of the synthesis concept of $NiCo_2S_4$ double-shell hollow sphere. (B, C) TEM images of 300 nm $NiCo_2S_4$ hollow sphere@SiO_2 core–shell structure. (D, E) TEM images of homogeneous $NiCo_2S_4$ double-shell hollow sphere with a shell thickness of around 150 nm.

$NiCo_2S_4$ phase for the NCS double-shell structure (Figure S12). To demonstrate the morphology-dependent improvement of electrochemical properties, the results of $NiCo_2S_4$ nanosheets (Figure S13) preparation based on commercial silica nanoparticle is included for comparison (see Experimental Section for details). The N_2 adsorption/desorption experiments were used to measure the surface area of nanosheets, single- and double-shell hollow spheres, which had a BET surface area of 29, 122, and 117 m^2 g^{-1}, respectively. Figure 5A,B shows the CV and CD profiles of NCS double-shell hollow spheres under different scan rates and current densities. They manifest similar redox peaks and distinct voltage plateaus as the single-shell NCS hollow spheres, suggesting analogous pseudocapacitive behavior. The CD profiles show highly symmetric features of the charge–discharge process, implying the high efficiency of $NiCo_2S_4$ electrode, excellent reversibility of redox reactions, and their superior rate capability. The anodic peaks shift to higher potential while the cathodic peaks shift to lower potential with increased scan rate due to the fast charge and discharge rates.[25] This yields wider potential difference between anodic and cathodic peaks, resulting in a capacitance decrease. Figure S14 demonstrates the linear relationship of anodic and cathodic peaks presented in Figure 5A versus the square root of scan rate, indicating the dominance of diffusion-controlled electrode reactions, which is one of the characteristics of pseudocapacitive materials.[43−45] Figure 5C shows CV curves of single- and double-shell NCS hollow spheres measured at the

DOI: 10.1021/acs.chemmater.5b01128
Chem. Mater. 2015, 27, 4661−4668

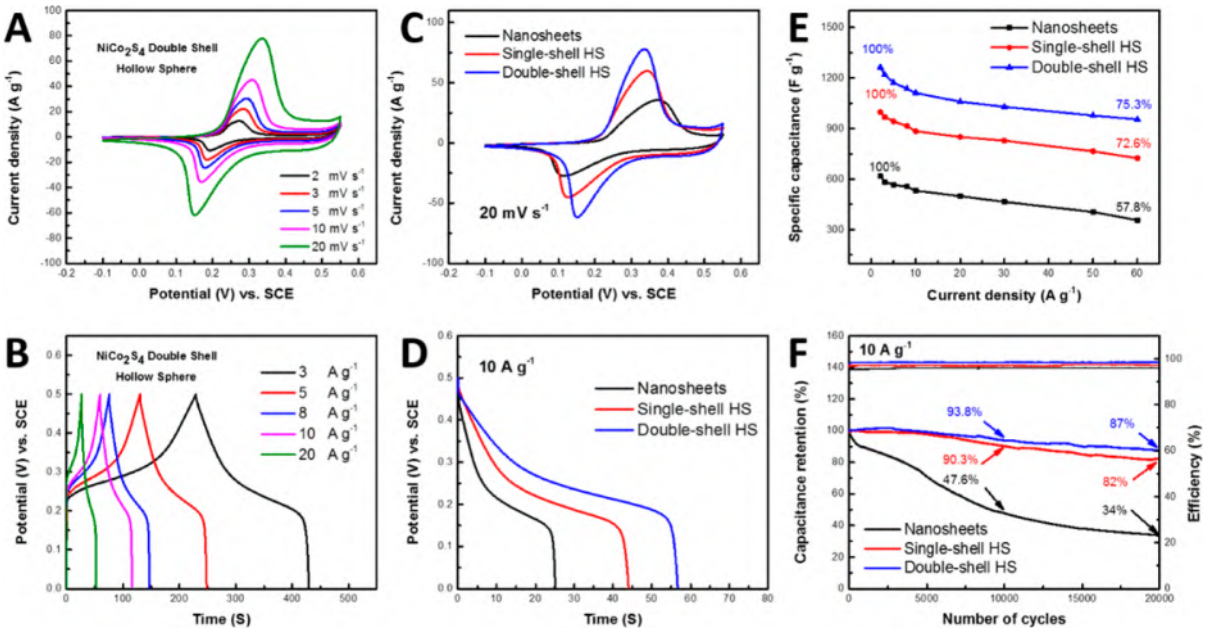

Figure 5. (A) Cyclic voltammetry and (B) galvanostatic charge−discharge profiles of $NiCo_2S_4$ double-shell hollow spheres (HS). (C) Comparison of cyclic voltammetry curves at the same scan rate of 20 mV s^{-1} and (D) galvanostatic discharge profiles at the same current density of 10 A g^{-1} of NCS nanosheets, single-shell HS, and double-shell HS. (E) Summary of specific capacitance and (F) cycling stability performance at current density of 10 A g^{-1} of NCS nanosheets, single-shell HS, and double-shell HS.

same scan rate of 20 mV s^{-1}. It can be clearly seen that the integrated area under the CV curve is higher for the double-shell NCS hollow spheres, meaning better electrochemical performance. Furthermore, the longer discharge period observed in Figure 5D of NCS double-shell hollow sphere confirms their better performance, a fact that is consistent with the results observed in the CV measurements. Figure 5E,F summarizes the detailed pseudocapacitive performance for the three products with different morphologies. It is evident that the double-shell NCS hollow spheres show the highest specific capacitance of 1263 F g^{-1} at 2 A g^{-1}, remarkable rate capability (75.3% retention of initial capacitance from 2 to 60 A g^{-1}), as well as superior cycling stability (93.8% and 87% capacitance retention after 10 000 and 20 000 cycles at a high current density of 10 A g^{-1}, respectively). These results are superior to those of the single-shell NCS hollow spheres and the NCS nanosheets. On the basis of the above impressive performance, especially the superlong cycle life which is comparable to that of carbonaceous materials, we can conclude that the $NiCo_2S_4$ with this unique structure is a promising material for next-generation pseudocapacitors.

To sum up, the NCS double-shell hollow spheres exhibit the best performance among the different $NiCo_2S_4$ morphologies studied in this work. Our performance is superior to that of all reported ternary nickel cobalt sulfides-based materials (literature reports are summarized in Table S1).[24,34,38,40,46−50] This phenomenon may be attributed to the unique double-shell structure which offers many desirable features. First of all, the highly porous double-shells surfaces are covered with self-assembled nanosheets which are full of mesopores (with size distribution centered around 3−5 nm, Figure S7B). These can provide a significant number of electroactive sites and shorter diffusion paths for charge transports, facilitating the redox reactions compared to their bulk or solid counterparts.[20] Besides, the nanometer-sized sheets are able to reduce diffusion time of the electrolyte ions, and can accommodate the strain during the OH^- insertion and extraction during electrochemical cycling.[51] Furthermore, the sacrificial-template growth process that we have developed results in robust adhesion between the inner and outer shells, leading to better stability during cycling. In addition, the NCS double-shell structure offers an impressively high surface area, suggesting the possibility of the exposure of numerous active sites available for reaction on the electrode surface.[40] Moreover, the higher meso-/macropore volume of double-shell NCS can boost the electrolyte ions trapping and access to the active sites. In addition, the vertically coated curved nanosheet arrays of the NCS double shells can increase the contact area between neighboring double shells (Figure S15) and provide a superb pathway for fast electron transportation through the electrodes.[25,52] Thus, we observed a higher electrical conductivity of NCS double shells (720 $\mu\Omega$ cm) over its single-shell counterparts (1600 $\mu\Omega$ cm). What's more, the void space in the hollow structure can better accommodate any volume change during cycling[53] and the thicker shell of the double-shell structure (150 vs 20 nm for single-shell 300 nm NCS) with high conductivity can more efficiently endure the extremely long cycling measurements, leading to better cycling performance as shown in Figure 5d (89% capacitance retention of NCS double shells vs 82% retention of 300 nm NCS single shells after 20 000 cycles). In contrast, the much poorer mechanical integrity of monodispersed or aggregated NCS nanosheets makes them pulverize more easily during electrochemical cycling, presenting unsatisfactory cycling stability (only 34% capacitance retention after 20 000 cycles). These results demonstrate that such the spherical double-shell construction of $NiCo_2S_4$ produces a pseudocapacitive material with superb performance.

4. CONCLUSION

In summary, we have demonstrated a facile hydrolysis−sulfidation strategy to fabricate well-defined $NiCo_2S_4$ hollow spheres with single- and double-shell configuration. The unique

DOI: 10.1021/acs.chemmater.5b01128
Chem. Mater. 2015, 27, 4661−4668

attributes of the double-shell hollow spheres include stable structure, high surface area, high permeability and void space, and remarkable pseudocapacitive performance in terms of ratability and extreme cycling stability. The cycling stability of our ternary chalcogenides is comparable to carbonaceous electrode materials, but with much higher specific capacitance (higher than any previously reported ternary chalcogenide), suggesting that these unique $NiCo_2S_4$ electrodes are promising pseudocapacitive materials for commercial applications. Importantly, this work also provides new insight into the controllable fabrication of mixed transition-metal chalcogenides with excellent properties.

■ ASSOCIATED CONTENT

Supporting Information

XRD, SEM, TEM, HAADF-STEM, XPS, EDS analysis, and BET measurements for precursor, single-shell, and double-shell $NiCo_2S_4$ are included. The Supporting Information is available free of charge on the ACS Publications website at DOI: 10.1021/acs.chemmater.5b01128.

■ AUTHOR INFORMATION

Corresponding Author

*E-mail: husam.alshareef@kaust.edu.sa.

Notes

The authors declare no competing financial interest.

■ ACKNOWLEDGMENTS

Research reported in this publication has been supported by King Abdullah University of Science and Technology (KAUST). The authors thank Dr. Peng Li, Dr. Rakhi RaghavanBaby, Dr. Narendra Kurra, and Bilal Ahmed at KAUST for several useful discussions. The authors thank the staff of the Imaging and Characterization Laboratory at KAUST, especially Dr. Nini Wei and Dr. Chao Zhao for their help with the TEM analysis and Dr. Nejib Hedhili for his help with the XPS measurements.

■ REFERENCES

(1) Simon, P.; Gogotsi, Y. Materials for electrochemical capacitors. *Nat. Mater.* **2008**, *7*, 845−854.

(2) Wang, K.; Wu, H. P.; Meng, Y. N.; Wei, Z. X. Conducting Polymer Nanowire Arrays for High Performance Supercapacitors. *Small* **2014**, *10*, 14−31.

(3) Xiong, P.; Liu, B.; Teran, V.; Zhao, Y.; Peng, L.; Wang, X.; Yu, G. Chemically Integrated Two-Dimensional Hybrid Zinc Manganate/Graphene Nanosheets with Enhanced Lithium Storage Capability. *ACS Nano* **2014**, *8*, 8610−8616.

(4) Xiong, P.; Peng, L.; Chen, D.; Zhao, Y.; Wang, X.; Yu, G. Two-dimensional nanosheets based Li-ion full batteries with high rate capability and flexibility. *Nano Energy* **2015**, *12*, 816−823.

(5) Armand, M.; Tarascon, J. M. Building better batteries. *Nature* **2008**, *451*, 652−657.

(6) Winter, M.; Brodd, R. J. What are batteries, fuel cells, and supercapacitors? *Chem. Rev.* **2005**, *105*, 1021−1021.

(7) Inagaki, M.; Konno, H.; Tanaike, O. Carbon materials for electrochemical capacitors. *J. Power Sources* **2010**, *195*, 7880−7903.

(8) Snook, G. A.; Kao, P.; Best, A. S. Conducting-polymer-based supercapacitor devices and electrodes. *J. Power Sources* **2011**, *196*, 1−12.

(9) Zhang, L. L.; Zhao, X. S. Carbon-based materials as supercapacitor electrodes. *Chem. Soc. Rev.* **2009**, *38*, 2520−2531.

(10) Rakhi, R. B.; Chen, W.; Cha, D.; Alshareef, H. N. Nanostructured Ternary Electrodes for Energy-Storage Applications. *Adv. Energy Mater.* **2012**, *2*, 381−389.

(11) Jiang, F. R.; Li, W. Y.; Zou, R. J.; Liu, Q.; Xu, K. B.; An, L.; Hu, J. Q. MoO_3/PANI coaxial heterostructure nanobelts by in situ polymerization for high performance supercapacitors. *Nano Energy* **2014**, *7*, 72−79.

(12) Chen, W.; Xia, C.; Rakhi, R. B.; Alshareerf, H. N. A general approach toward enhancement of pseudocapacitive performance of conducting polymers by redox-active electrolytes. *J. Power Sources* **2014**, *267*, 521−526.

(13) Zhang, X.; Zeng, X. Z.; Yang, M.; Qi, Y. X. Investigation of a Branchlike MoO3/Polypyrrole Hybrid with Enhanced Electrochemical Performance Used as an Electrode in Supercapacitors. *ACS Appl. Mater. Interfaces* **2014**, *6*, 1125−1130.

(14) Dong, X. L.; Guo, Z. Y.; Song, Y. F.; Hou, M. Y.; Wang, J. Q.; Wang, Y. G.; Xia, Y. Y. Flexible and Wire-Shaped Micro-Supercapacitor Based on $Ni(OH)_2$-Nanowire and Ordered Mesoporous Carbon Electrodes. *Adv. Funct Mater.* **2014**, *24*, 3405−3412.

(15) Wang, G. P.; Zhang, L.; Zhang, J. J. A review of electrode materials for electrochemical supercapacitors. *Chem. Soc. Rev.* **2012**, *41*, 797−828.

(16) Yan, J.; Wang, Q.; Wei, T.; Fan, Z. J. Recent Advances in Design and Fabrication of Electrochemical Supercapacitors with High Energy Densities. *Adv. Energy Mater.* **2014**, *4*, 1300816.

(17) Wan, H. Z.; Ji, X.; Jiang, J. J.; Yu, J. W.; Miao, L.; Zhang, L.; Bie, S. W.; Chen, H. C.; Ruan, Y. J. Hydrothermal synthesis of cobalt sulfide nanotubes: The size control and its application in supercapacitors. *J. Power Sources* **2013**, *243*, 396−402.

(18) Apostolova, R. D.; Shembel, E. M.; Talyosef, I.; Grinblat, J.; Markovsky, B.; Aurbach, D. Study of electrolytic cobalt sulfide Co_9S_8 as an electrode material in lithium accumulator prototypes. *Russ J. Electrochem+* **2009**, *45*, 311−319.

(19) Peng, S. J.; Li, L. L.; Tan, H. T.; Cai, R.; Shi, W. H.; Li, C. C.; Mhaisalkar, S. G.; Srinivasan, M.; Ramakrishna, S.; Yan, Q. Y. MS 2 (M = Co and Ni) Hollow Spheres with Tunable Interiors for High-Performance Supercapacitors and Photovoltaics. *Adv. Funct Mater.* **2014**, *24*, 2155−2162.

(20) Zhu, T.; Wang, Z. Y.; Ding, S. J.; Chen, J. S.; Lou, X. W. Hierarchical nickel sulfide hollow spheres for high performance supercapacitors. *RSC Adv.* **2011**, *1*, 397−400.

(21) Yang, Z. S.; Chen, C. Y.; Chang, H. T. Supercapacitors incorporating hollow cobalt sulfide hexagonal nanosheets. *J. Power Sources* **2011**, *196*, 7874−7877.

(22) Shen, L.; Yu, L.; Wu, H. B.; Yu, X.-Y.; Zhang, X.; Lou, X. W. D. Formation of nickel cobalt sulfide ball-in-ball hollow spheres with enhanced electrochemical pseudocapacitive properties. *Nat. Commun.* **2015**, *6*.

(23) Xiao, J. W.; Wan, L.; Yang, S. H.; Xiao, F.; Wang, S. Design Hierarchical Electrodes with Highly Conductive $NiCo_2S_4$ Nanotube Arrays Grown on Carbon Fiber Paper for High-Performance Pseudocapacitors. *Nano Lett.* **2014**, *14*, 831−838.

(24) Pu, J.; Cui, F. L.; Chu, S. B.; Wang, T. L.; Sheng, E. H.; Wang, Z. H. Preparation and Electrochemical Characterization of Hollow Hexagonal $NiCo_2S_4$ Nanoplates as Pseudocapacitor Materials. *ACS Sustain. Chem. Eng.* **2014**, *2*, 809−815.

(25) Chen, W.; Xia, C.; Alshareef, H. N. One-Step Electrodeposited Nickel Cobalt Sulfide Nanosheet Arrays for High-Performance Asymmetric Supercapacitors. *ACS Nano* **2014**, *8*, 9531−9541.

(26) Chen, H. C.; Jiang, J. J.; Zhang, L.; Xia, D. D.; Zhao, Y. D.; Guo, D. Q.; Qi, T.; Wan, H. Z. In situ growth of NiCo2S4 nanotube arrays on Ni foam for supercapacitors: Maximizing utilization efficiency at high mass loading to achieve ultrahigh areal pseudocapacitance. *J. Power Sources* **2014**, *254*, 249−257.

(27) Shao, M. F.; Ning, F. Y.; Zhao, Y. F.; Zhao, J. W.; Wei, M.; Evans, D. G.; Duan, X. Core-Shell Layered Double Hydroxide Microspheres with Tunable Interior Architecture for Supercapacitors. *Chem. Mater.* **2012**, *24*, 1192−1197.

(28) Lou, X. W.; Li, C. M.; Archer, L. A. Designed Synthesis of Coaxial SnO_2@carbon Hollow Nanospheres for Highly Reversible Lithium Storage. *Adv. Mater.* **2009**, *21*, 2536.

DOI: 10.1021/acs.chemmater.5b01128
Chem. Mater. 2015, 27, 4661−4668

(29) Xu, H. L.; Wang, W. Z. Template synthesis of multishelled Cu_2O hollow spheres with a single-crystalline shell wall. *Angew. Chem., Int. Ed.* **2007**, *46*, 1489−1492.
(30) Stober, W.; Fink, A.; Bohn, E. Controlled Growth of Monodisperse Silica Spheres in Micron Size Range. *J. Colloid Interface Sci.* **1968**, *26*, 62.
(31) Li, W.; Deng, Y. H.; Wu, Z. X.; Qian, X. F.; Yang, J. P.; Wang, Y.; Gu, D.; Zhang, F.; Tu, B.; Zhao, D. Y. Hydrothermal Etching Assisted Crystallization: A Facile Route to Functional Yolk-Shell Titanate Microspheres with Ultrathin Nanosheets-Assembled Double Shells. *J. Am. Chem. Soc.* **2011**, *133*, 15830−15833.
(32) V, K.; Frackowiak, E.; Beguin, F. Determination of the specific capacitance of conducting polymer/nanotubes composite electrodes using different cell configurations. *Electrochim. Acta* **2005**, *50*, 2499−2506.
(33) Jin, P.; Chen, Q. W.; Hao, L. Q.; Tian, R. F.; Zhang, L. X.; Wang, L. Synthesis and catalytic properties of nickel-silica composite hollow nanospheres. *J. Phys. Chem. B* **2004**, *108*, 6311−6314.
(34) Yu, L.; Zhang, L.; Wu, H. B.; Lou, X. W. Formation of $NixCo_3$-xS_4 Hollow Nanoprisms with Enhanced Pseudocapacitive Properties. *Angew. Chem., Int. Ed.* **2014**, *53*, 3711−3714.
(35) Kim, W. S.; Hwa, Y.; Jeun, J. H.; Sohn, H. J.; Hong, S. H. Synthesis of SnO_2 nano hollow spheres and their size effects in lithium ion battery anode application. *J. Power Sources* **2013**, *225*, 108−112.
(36) Balaya, P. Size effects and nanostructured materials for energy applications. *Energy Environ. Sci.* **2008**, *1*, 645−654.
(37) Chen, X. Y.; Zhu, H. L.; Chen, Y. C.; Shang, Y. Y.; Cao, A. Y.; Hu, L. B.; Rubloff, G. W. MWCNT/V_2O_5 Core/Shell Sponge for High Areal Capacity and Power Density Li-Ion Cathodes. *ACS Nano* **2012**, *6*, 7948−7955.
(38) Chen, H. C.; Jiang, J. J.; Zhang, L.; Wan, H. Z.; Qi, T.; Xia, D. D. Highly conductive $NiCo_2S_4$ urchin-like nanostructures for high-rate pseudocapacitors. *Nanoscale* **2013**, *5*, 8879−8883.
(39) Mei, L.; Yang, T.; Xu, C.; Zhang, M.; Chen, L. B.; Li, Q. H.; Wang, T. H. Hierarchical mushroom-like $CoNi_2S_4$ arrays as a novel electrode material for supercapacitors. *Nano Energy* **2014**, *3*, 36−45.
(40) Zhu, Y. R.; Wu, Z. B.; Jing, M. J.; Yang, X. M.; Song, W. X.; Ji, X. B. Mesoporous $NiCo_2S_4$ nanoparticles as high-performance electrode materials for supercapacitors. *J. Power Sources* **2015**, *273*, 584−590.
(41) Shan, Z. W.; Adesso, G.; Cabot, A.; Sherburne, M. P.; Asif, S. A. S.; Warren, O. L.; Chrzan, D. C.; Minor, A. M.; Alivisatos, A. P. Ultrahigh stress and strain in hierarchically structured hollow nanoparticles. *Nat. Mater.* **2008**, *7*, 947−952.
(42) Yao, Y.; McDowell, M. T.; Ryu, I.; Wu, H.; Liu, N. A.; Hu, L. B.; Nix, W. D.; Cui, Y. Interconnected Silicon Hollow Nanospheres for Lithium-Ion Battery Anodes with Long Cycle Life. *Nano Lett.* **2011**, *11*, 2949−2954.
(43) Luo, F. L.; Li, J.; Yuan, H. Y.; Xiao, D. Rapid synthesis of three-dimensional flower-like cobalt sulfide hierarchitectures by microwave assisted heating method for high-performance supercapacitors. *Electrochim. Acta* **2014**, *123*, 183−189.
(44) Kim, H.; Park, K. Y.; Hong, J.; Kang, K. All-graphene-battery: bridging the gap between supercapacitors and lithium ion batteries. *Sci. Rep.* **2014**, *4*, 5278.
(45) Chen, K. F.; Song, S. Y.; Li, K. Y.; Xue, D. F. Water-soluble inorganic salts with ultrahigh specific capacitance: crystallization transformation investigation of CuCl2 electrodes. *CrystEngComm* **2013**, *15*, 10367−10373.
(46) Zhang, Y. F.; Ma, M. Z.; Yang, J.; Sun, C. C.; Su, H. Q.; Huang, W.; Dong, X. C. Shape-controlled synthesis of $NiCo_2S_4$ and their charge storage characteristics in supercapacitors. *Nanoscale* **2014**, *6*, 9824−9830.
(47) Yang, J. Q.; Guo, W.; Li, D.; Qin, Q.; Zhang, J.; Wei, C. Y.; Fan, H. M.; Wu, L. Y.; Zheng, W. J. Hierarchical porous $NiCo_2S_4$ hexagonal plates: Formation via chemical conversion and application in high performance supercapacitors. *Electrochim. Acta* **2014**, *144*, 16−21.
(48) Pu, J.; Wang, T. T.; Wang, H. Y.; Tong, Y.; Lu, C. C.; Kong, W.; Wang, Z. H. Direct Growth of $NiCo_2S_4$ Nanotube Arrays on Nickel Foam as High-Performance Binder-Free Electrodes for Supercapacitors. *ChemPlusChem* **2014**, *79*, 577−583.
(49) Wan, H. Z.; Jiang, J. J.; Yu, J. W.; Xu, K.; Miao, L.; Zhang, L.; Chen, H. C.; Ruan, Y. J. $NiCo_2S_4$ porous nanotubes synthesis via sacrificial templates: high-performance electrode materials of supercapacitors. *CrystEngComm* **2013**, *15*, 7649−7651.
(50) Peng, S. J.; Li, L. L.; Li, C. C.; Tan, H. T.; Cai, R.; Yu, H.; Mhaisalkar, S.; Srinivasan, M.; Ramakrishna, S.; Yan, Q. Y. In situ growth of $NiCo_2S_4$ nanosheets on graphene for high-performance supercapacitors. *Chem. Commun.* **2013**, *49*, 10178−10180.
(51) Wang, X.; Wu, X. L.; Guo, Y. G.; Zhong, Y. T.; Cao, X. Q.; Ma, Y.; Yao, J. N. Synthesis and Lithium Storage Properties of Co_3O_4 Nanosheet-Assembled Multishelled Hollow Spheres. *Adv. Funct. Mater.* **2010**, *20*, 1680−1686.
(52) Li, H. B.; Yu, M. H.; Wang, F. X.; Liu, P.; Liang, Y.; Xiao, J.; Wang, C. X.; Tong, Y. X.; Yang, G. W. Amorphous nickel hydroxide nanospheres with ultrahigh capacitance and energy density as electrochemical pseudocapacitor materials. *Nat. Commun.* **2013**, *4*.
(53) Taberna, L.; Mitra, S.; Poizot, P.; Simon, P.; Tarascon, J. M. High rate capabilities Fe_3O_4-based Cu nano-architectured electrodes for lithium-ion battery applications. *Nat. Mater.* **2006**, *5*, 567−573.

DOI: 10.1021/acs.chemmater.5b01128
Chem. Mater. 2015, 27, 4661−4668